RSC Applied Polymers

ROYAL SOCIETY OF CHEMISTRY

PAPER

View Article Online
View Journal | View Issue

Cite this: *RSC Appl. Polym.*, 2025, **3**, 1278

Development of poly(ρ-coumaric acid) based nanodrug delivery system incorporating hyaluronic acid for enhanced wound healing†

Siying Wu,‡[a] Mengfang Yuan,‡[a] Shuyan Han,[b] Liying Wang,*[a] Xinru You*[c] and Jun Wu *[a,d]

Wound healing is a multifaceted physiological process, often hindered by persistent inflammation, homeostatic imbalance, and impaired tissue regeneration. Traditional therapies frequently fall short in addressing these challenges, underscoring the need for advanced therapeutic strategies. In this study, we designed a novel nanodrug delivery system based on poly(ρ-coumaric acid) (PCA), a bioactive polymer derived from natural sources, known for its anti-inflammatory and antioxidant properties. The PCA nanoparticles (NPs) were engineered to encapsulate ibuprofen (IBP), a non-steroidal anti-inflammatory drug, and subsequently integrated with hyaluronic acid (HA) to enhance wound site adhesion and create a moist regenerative microenvironment. This multifunctional platform (PCA@IBP NPs/HA) could synergistically achieve sustained drug release and leverage the intrinsic bioactivity of its components. *In vitro* assays demonstrated that the system effectively promoted cell migration and angiogenesis due to the combined anti-inflammatory effects. *In vivo* studies using an acute wound model confirmed accelerated wound closure, superior re-epithelialization, and collagen deposition. This work provided a novel strategy that synergistically integrated traditional herbal bioactive with nanotechnology, offering a promising platform for the development of next-generation wound-healing therapeutics.

Received 11th April 2025,
Accepted 21st June 2025

DOI: 10.1039/d5lp00107b

rsc.li/rscapplpolym

1 Introduction

Wound healing is a complex process consisting of four major stages, which are usually prone to stall in the inflammatory phase. Effective wound management plays a critical role in restoring both structural integrity and physiological function in complex wound healing. However, current clinical approaches demonstrate suboptimal efficacy, for example conventional biochemical interventions (such as growth factor applications) and standard biophysical modalities (including basic debridement procedures or negative pressure wound therapy) frequently yield inadequate therapeutic results for chronic wound treatment.[1,2] These traditional therapeutic approaches often fall short in addressing the unique demands of the wounds, characterized by prolonged inflammation, cellular dysfunction, and impaired tissue regeneration.[3,4] Therefore, growing demands of advanced therapeutic systems have emerged to address the intricate microenvironment of wounds, ultimately improving healing outcomes and reducing patient suffering.[5–7] Recently, natural compounds derived from Chinese medicinal herbs have gained significant attention due to their excellent biocompatibility and inherent bioactivities, including anti-inflammatory, antioxidant, and regenerative effects.[8–10] Different from the structural singularity of general natural biomaterials and the limitations of synthetic biomaterials in terms of function and bioactivity, polymeric biomaterials based on active ingredients of Chinese herbal medicine have shown some significant advantages in the application of nanodrug delivery systems. These natural compounds offer a promising foundation for developing multifunctional biomaterials that serve not only as drug carriers but also as active participants in the treatment process.[11–13]

Herein, a poly(ρ-coumaric acid) (PCA)-based nanodrug delivery system encapsulating with ibuprofen (IBP) and combined with hyaluronic acid (HA) was developed as PCA@IBP

[a]*Bioscience and Biomedical Engineering Thrust, The Hong Kong University of Science and Technology (Guangzhou), Nansha, Guangzhou, 511400 Guangdong, China. E-mail: wangly53@mail2.sysu.edu.cn, junwuhkust@ust.hk*
[b]*Department of Nephrology, Center of Kidney and Urology, The Seventh Affiliated Hospital, Sun Yat-Sen University, Shenzhen, 518107, China*
[c]*Center for Nanomedicine and Department of Anesthesiology, Brigham and Women's Hospital, Harvard Medical School, Boston, MA 02115, USA. E-mail: xyou2@bwh.harvard.edu*
[d]*Division of Life Science, The Hong Kong University of Science and Technology, Hong Kong, SAR, 999077, China*

†Electronic supplementary information (ESI) available. See DOI: https://doi.org/10.1039/d5lp00107b

‡These two authors contributed equally to this work.

NPs/HA for the treatment of acute wounds. The ρ-coumaric acid, a bioactive molecule derived from natural sources, exhibits anti-inflammatory and antioxidant properties, making it an appropriate candidate for enhancing wound healing.[14–16] Through a one-step polycondensation reaction, ρ-coumaric acid was synthesized into PCA, a biocompatible and bioactive polymer capable of self-assembling into nanoparticles (PCA NPs). Additionally, the PCA NPs could further serve as carriers for loading, delivery and controlled release of active pharmaceutical ingredients to synergistically facilitate wound healing. The IBP was then selected to establish nanodrug systems. As known, IBP is a widely used non-steroidal anti-inflammatory drug to mitigate acute inflammation and alleviate pain at the disease site, which makes it a promising candidate for enhancing wound healing through inflammation modulation and pain management. However, its clinical translation in wound care faces significant challenges due to its short half-life, high hydrophobicity and serious adverse effects after conventional frequent high-dose systemic administration.[17–20] Therefore, a controlled and sustained-release system for topical IBU delivery is acknowledged as an appropriate alternative to enhance therapeutic efficacy, which could improve the IBP stability and accessibility to the wound region and also reduce systemic exposure. Nanodrug delivery systems platforms offer more possibilities *via* effective drug encapsulation, controlled drug release, and enhanced drug bioavailability.[21–23] By combining traditional herbal medicine with advanced nanotechnology, it is possible to create novel therapeutic strategy that leverage the wound healing potential of these bioactive compounds. The incorporation of HA with the PCA@IBP NPs further enhanced the therapeutic potential of this combined platform.[24,25] HA, a naturally occurring polysaccharide, not only improved the bioadhesion and retention of the PCA@IBP NPs at the wound site but also provided a moist environment conducive to tissue regeneration.[26–28] The combination of PCA@IBP NPs with HA could effectively achieve sustained nanodrug release, prolonging the therapeutic effects of IBP and maximizing the benefits of the bioactive PCA polymers.

The PCA polymeric nanocarriers with additional self-therapeutic properties exerted a regulatory effect synergistic with the loading drugs. *In vitro* studies indicated that PCA@IBP NPs effectively improve skin cell activity and functionality promoting cell migration and angiogenesis due to their enhanced anti-inflammatory capacity. *In vivo* experiments further confirmed that PCA@IBP NPs/HA accelerated wound closure, optimized re-epithelialization, and collagen deposition in acute wound models, suggesting its potential as a powerful wound-healing agent. This study developed an innovative approach and strategy to accelerative wound healing *via* combining the bioactive properties of natural compounds with advanced nanodrug delivery systems. By leveraging the dual therapeutic effects of PCA and IBP, along with the enhanced retention provided by HA, this multifunctional system contributed to the development of advanced hybrid biomaterials for addressing the complex demands during wound healing (Scheme 1).

2 Results and discussion

2.1 Preparation and characterization of PCA NPs and PCA@IBP NPs

The PCA polymer was produced through a one-step polycondensation reaction using ρ-coumaric acid. The chemical structure of PCA was characterized by ^{1}H-nuclear magnetic resonance (^{1}H-NMR) and Fourier transform infrared (FT-IR) spectra in the ESI (Fig. S1 and S2†), confirming the successful polymerization. The gel permeation chromatography (GPC) was then used to measure the molecular weight of the PCA polymer, as depicted in Fig. S3.† In Table S1,† it indicated that the Mw of PCA polymer was 9223, with a PDI of 1.4651, indicating that the polymerization reaction resulted in approximately 43 repeating units in the polymer chain.

The PCA NPs and PCA@IBP NPs were prepared using the nanoprecipitation method. The ratio of drug to carrier, along with the proportion of organic (oil) phase to aqueous (water) phase, are critical factors that influence encapsulation efficiency (EE%) and drug loading (DL%). In this study, the ratio of the oil phase to the water phase was fixed at 1 : 10, while different ratios of IBP to PCA polymer were explored to optimize the EE% and DL% of the nanoparticles (Table S2†). An HPLC-based standard curve for IBP was established to quantify EE% and DL% of PCA@IBP NPs at different ratios. The EE% and DL% were measured for each ratio, allowing the identification of the most suitable IBP-to-PCA ratio for screening the optimal nanoparticle formation. As shown in Table S2,† when the ratio of PCA to IBP was 5 : 1, the PCA@IBP NPs exhibited the highest drug loading capacity (4.14%) and encapsulation efficiency (26.47%). Therefore, this ratio was selected for use in subsequent experiments.

The prepared PCA NPs and PCA@IBP NPs were illustrated in Fig. 1a. Both of them appeared as uniform, transparent, light brown solutions and exhibited the Tyndall effect, indicating the presence of well-dispersed nanoparticles in the solution. Subsequently, the particle size of PCA NPs and PCA@IBP NPs was measured using dynamic light scattering (DLS), which was 128.2 ± 4.7 nm and 135.3 ± 1.8 nm, respectively, with PDI of 0.163 ± 0.051 and 0.106 ± 0.066 (Fig. 1b). The morphology of PCA NPs and PCA@IBP NPs was further characterized using transmission electron microscopy (TEM). As shown in the Fig. 1d, both PCA NPs and PCA@IBP NPs displayed a spherical shape with high sphericity, confirming their well-defined nanosphere morphology.

The stability of a nanodrug delivery platform is crucial for its effectiveness. Therefore, the stability of PCA@IBP NPs in PBS (pH 7.4) and PBS containing 10% FBS was assessed for 7 days. As shown in Fig. 1c, the particle size of NPs hardly changed in both PBS (pH 7.4) that mimics the pH of the physiological environment and PBS containing 10% FBS that mimics the environment when blood circulation during the test period, with size fluctuating between 120–140 nm. It demonstrated the excellent stability of PCA@IBP NPs under physiological conditions. After that, the release profile of IBP from PCA@IBP NPs was evaluated under pH 7.4 and pH 8.4

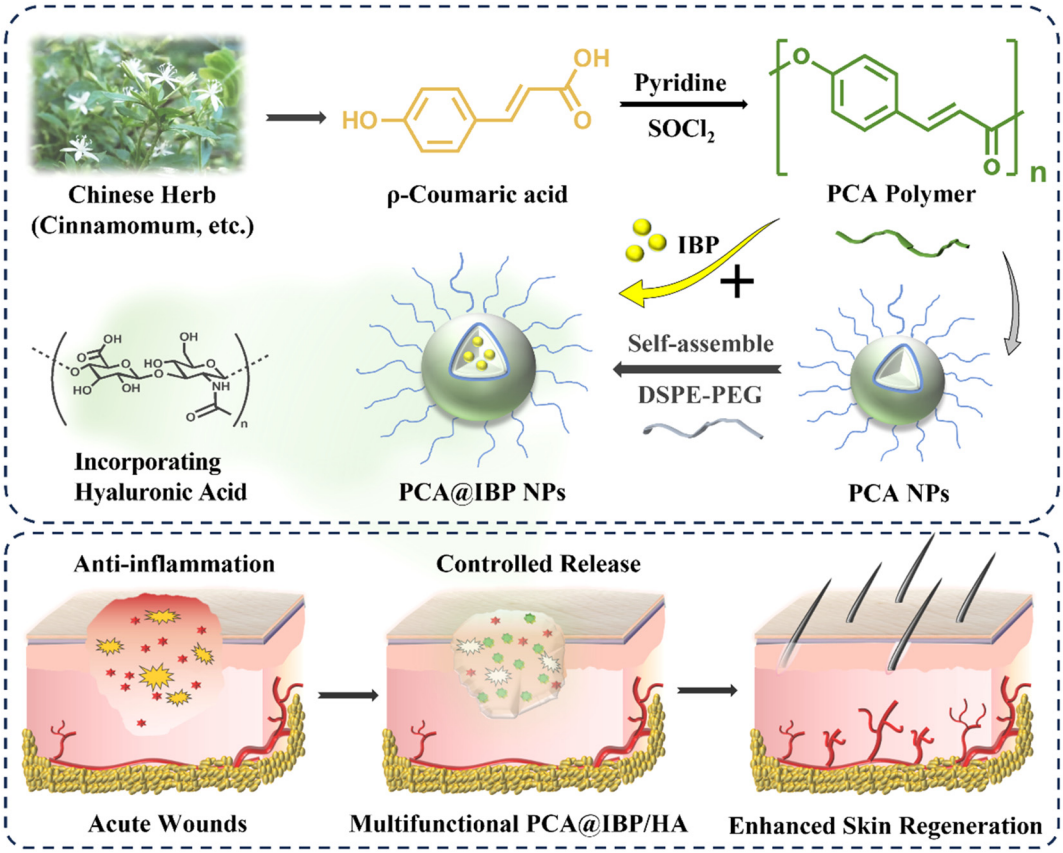

Scheme 1 The ibuprofen (IBP) encapsulated poly(ρ-coumaric acid) (PCA) nanodrug delivery systems incorporating hyaluronic acid (HA) for enhanced wound healing.

conditions. A pH of 7.4 closely mimicked normal physiological conditions, while pH 8.4 represented the alkaline environment typical of wound microenvironment. The standard curve for IBP was established using HPLC. As shown in Fig. 1e, a rapid drug release (over 35%) was observed within the first 12 h, which was beneficial for making rapid anti-inflammatory effects at acute wound sites. Following this initial burst, the PCA NPs exhibited a more sustained release behavior, indicating their potential for long-term anti-inflammatory activity through controlled drug delivery.

2.2 *In vitro* biocompatibility and cellular uptake of PCA@IBP NPs

The *in vitro* hemolysis assay evaluates the integrity of the red blood cell (RBC) membrane by measuring the release of hemoglobin from RBCs. As shown in Fig. 1f, after co-incubating different concentrations of PCA@IBP NPs with RBCs for 3 h and centrifuging the samples, the supernatant remained clear, suggesting no RBC lysis. The hemolysis rate was calculated to be below 5% (Fig. 1g). Although PCA@IBP NPs presented inherent color, the color of the supernatant after centrifugation with RBCs was consistent with the supernatant from the group without RBCs, confirming that the color of PCA@IBP NPs did not interfere with the results.

Cytotoxicity assay and live/dead staining were conducted for evaluating the cytocompatibility of nanodrug delivery systems. Both the methylthiazolyldiphenyl-tetrazolium bromide (MTT) assay and 5-ethynyl-2′-deoxyuridine (EdU) assay were used to assess the cell viability of PCA NPs and PCA@IBP NPs. The results in Fig. 2a and Fig. S4† indicated that NPs showed good cytocompatibility to NIH 3T3 cells and cells treated with varying concentrations of NPs could maintain metabolic activity without significant cytotoxicity.

Live/dead staining was then performed using calcein-AM and PI to stain live cells with green fluorescence and dead cells with red fluorescence. In Fig. 2d, NIH 3T3 cells treated with PCA NPs and PCA@IBP NPs displayed significant green fluorescence intensity aligning with the control group, with only minimal red fluorescence observed. The high cell survival rate was visualized in all experimental groups, further confirming the desirable biocompatibility of NPs. These findings all verified that the potential of PCA NPs and PCA@IBP NPs as valuable candidates for wound dressings.

Since most nanodrug delivery systems exert their therapeutic effects through intracellular uptake, the cellular internalization of PCA NPs was further investigated by both qualitative analyses using an inverted fluorescence microscope and quantitative analyses using flow cytometry. As indicated in

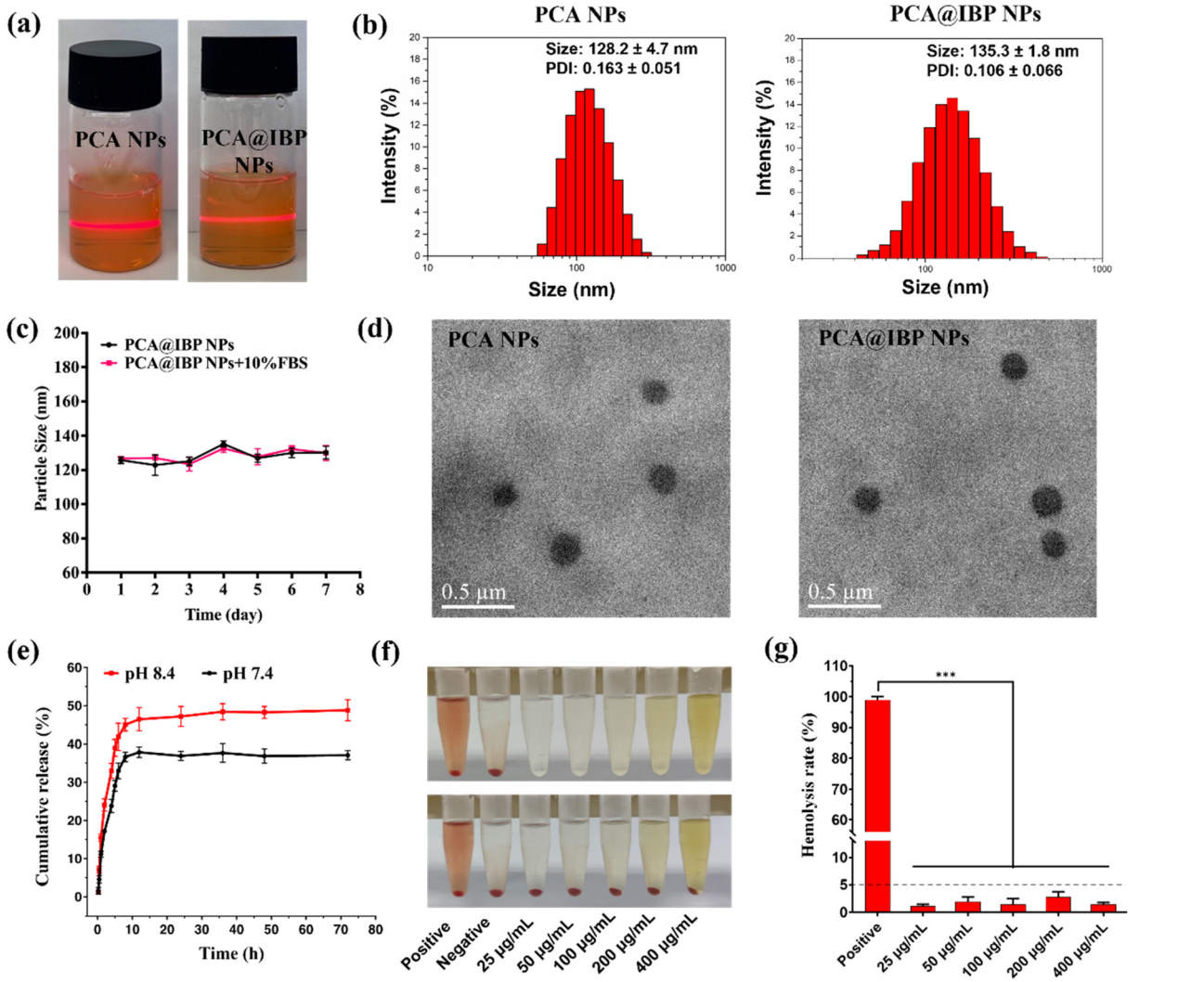

Fig. 1 Preparation and characterization of PCA NPs and PCA@IBP NPs. (a) Photograph of the PCA NPs and PCA@IBP NPs with Tyndall effect. (b) Particle size and distribution of PCA NPs and PCA@IBP NPs. (c) Stability of PCA@IBP NPs (n = 3). (d) TEM image of PCA NPs and PCA@IBP NPs. (e) *In vitro* release profiles of IBP from PCA@IBP NPs in pH condition at 7.4 and 8.4 (n = 3). (f) Representative images of hemolysis with (down) or without (up) red blood cells after treated with water (positive), saline (negative), and different concentrations of PCA NPs. (g) Hemolysis ratio analysis based on (e) (n = 3).

Fig. 2e, after co-incubation with PCA@C6 NPs for several hours, the intracellular green fluorescence intensity increased significantly over time, suggesting that the PCA NPs could be absorbed by cells and it was in a time-dependent manner. The flow cytometry results further confirmed the observation, showing a progressive increase in fluorescence intensity with extended incubation times, consistent with the results observed under the fluorescence microscope (Fig. 2b and c).

2.3 *In vitro* anti-inflammatory properties of PCA@IBP NPs

Macrophages are essential to the wound healing process, as they regulate the inflammatory response and facilitate tissue repair. In this study, the PCA nanocarriers based on natural Chinese herbal medicine possessed inherent anti-inflammatory ability. By further loading anti-inflammatory small molecule drugs, it could be expected to achieve a regulatory effect on the inflammatory microenvironment that is greater than the sum of its parts.[29–31] The downregulation of the local high inflammatory levels was important for alleviating the damaged vitality of cells and thereby promoting more efficient wound healing. Therefore, to examine the anti-inflammatory properties of PCA@IBP NPs, macrophages were served as models. The focus of this analysis was to determine how PCA@IBP NPs influenced macrophage activity, particularly in modulating the release of pro-inflammatory cytokines after the effective cellular uptake of free drugs or bioactive NPs. RT-PCR was employed to detect the mRNA expression levels of IL-6, IL-1β, TNF-α, and iNOS in macrophages (Fig. 3a–c and Fig. S5†). The results demonstrated that IBP, PCA NPs and PCA@IBP NPs treatments groups effectively suppressed the fold change of

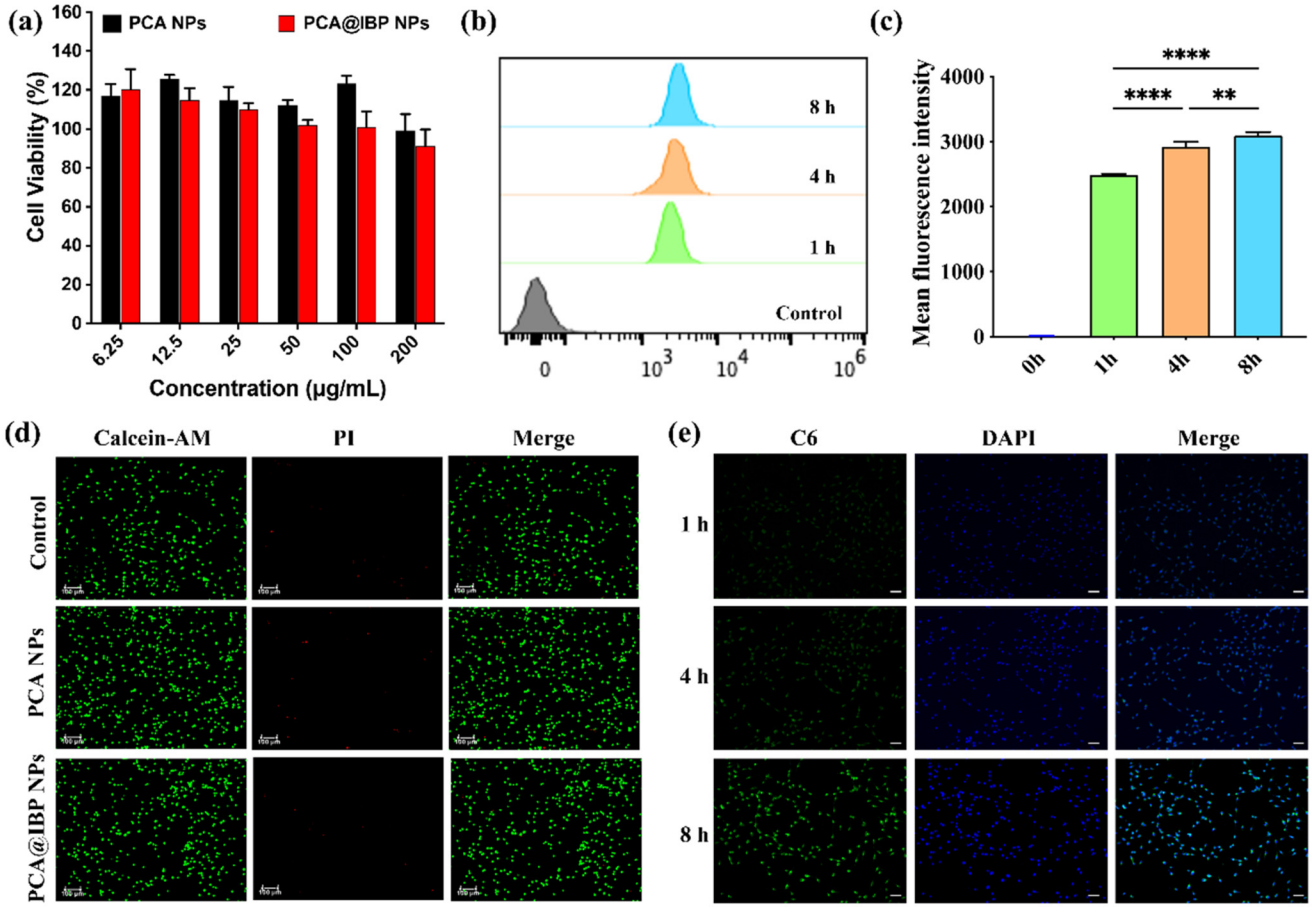

Fig. 2 *In vitro* cellular compatibility and cellular uptake of PCA@IBP NPs. (a) Cell viability of NIH 3T3 cells treated with PCA NPs or PCA@IBP NPs at different concentrations for 24 h by MTT assays (n = 3). (b) Flow cytometry and (c) quantitative analysis of the cellular uptake of PCA@C6 NPs on NIH 3T3 cells for different time (n = 3). (d) Representative live/dead cell staining images after various treatments. Scale bar, 100 μm. (e) Cellular uptake images of NIH 3T3 cells treated with PCA@C6 NPs for different times. Scale bar, 100 μm. $^{**}p < 0.01$, $^{****}p < 0.0001$.

pro-inflammatory cytokines as compared to LPS-stimulated positive groups. Moreover, in comparison to the IBP group, PCA NPs and PCA@IBP NPs exhibited a more pronounced downregulation of these cytokines. This phenomenon confirmed the remarkable anti-inflammatory property of PCA itself. Additionally, the anti-inflammatory effects were also evaluated through ELISA assays (Fig. 3d–f). Consistent with the RT-PCR data, the secretion of inflammatory factors indicated that both PCA NPs and PCA@IBP NPs lowered the levels of pro-inflammatory cytokines in macrophages. All these results indicated that PCA NPs, either alone or combined with IBP, could play a potent anti-inflammatory role for enhanced wound healing.

2.4 *In vitro* cell migration and angiogenesis promotion of PCA@IBP NPs

Given the ability of PCA NPs and PCA@IBP NPs to maintain and enhance skin cell activity and reverse the inflammatory microenvironment, an *in vitro* scratch assay was employed to evaluate the effect of PCA@IBP NPs on enhancing cell migration.[32,33] The representative images of cell migration after various treatments were shown in Fig. 4a with the semi-quantitative data of healing rates at different time point calculated in Fig. 4b–e. The results demonstrated that IBP group and PCA NPs group displayed similar levels of wound healing at 8 h, showing no statistically meaningful differences compatible to control. At 16 h, the PCA NPs and PCA@IBP NPs groups showed a notable improvement in wound healing as compared to the control, indicating a significant effect on cell migration. At 24 and 48 h, the PCA@IBP NPs group exhibited the highest percentage of wound healing, with statistically significant differences from the control and IBP groups. Meanwhile, PCA NPs also presented a significant impact, albeit lower than PCA@IBP NPs did. The IBP group exhibited a notable difference in wound healing only at 48 h, while no significant differences were observed at earlier time points. These findings suggested that both PCA NPs and PCA@IBP NPs were effective in promoting cell migration and wound healing, with PCA@IBP NPs demonstrating superior efficacy, particularly at later time points. The sustained increase in healing percentage for PCA@IBP NPs indicated the potential of the nanodrug delivery system for facilitating wound repair processes.

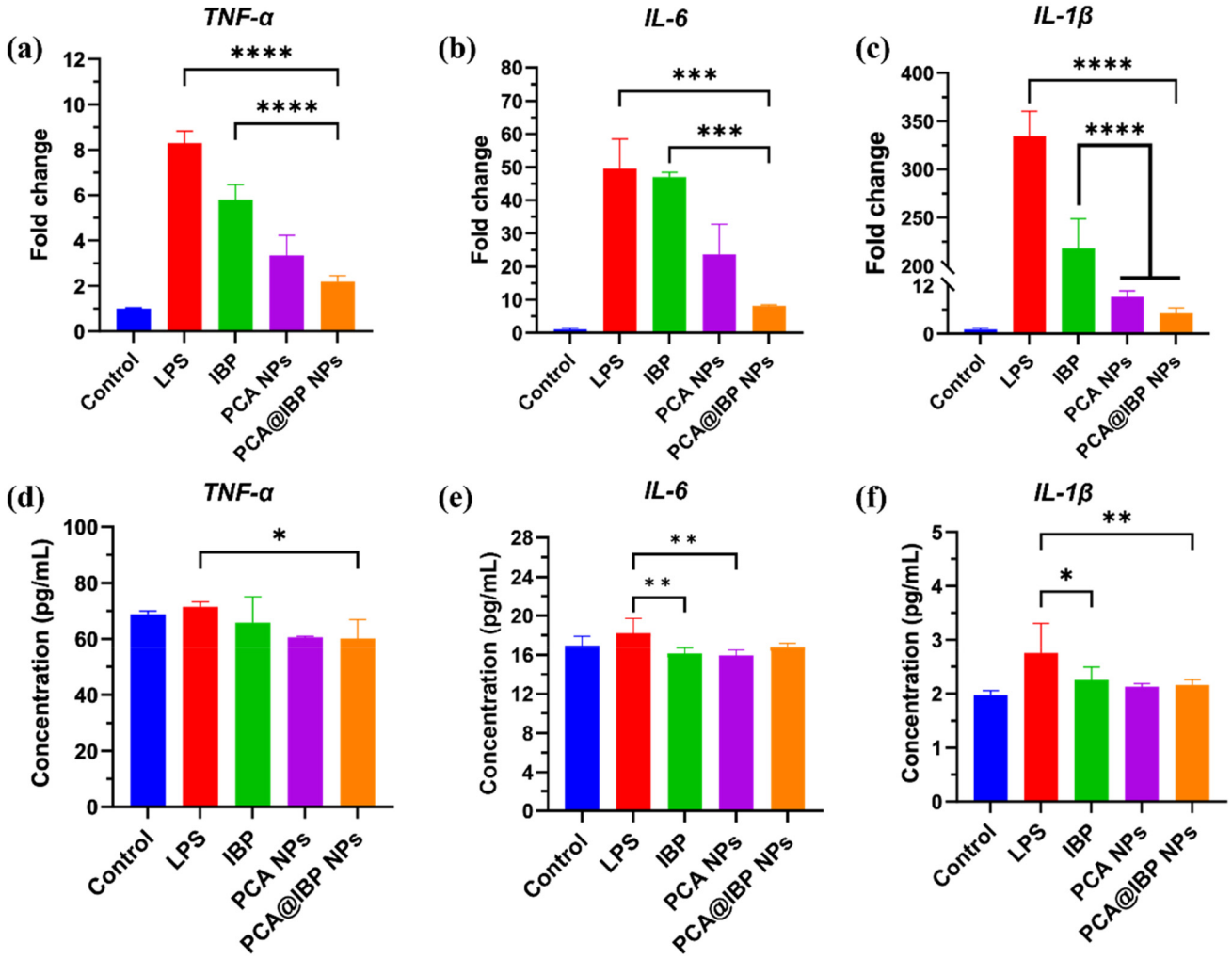

Fig. 3 *In vitro* anti-inflammatory properties of PCA@IBP NPs. The mRNA expression of TNF-α (a), IL-6 (b), and IL-1β (c) in LPS-activated RAW 264.7 cells treated with IBP, PCA NPs or PCA@IBP NPs (n = 3). Concentration of TNF-α (d), IL-6 (e), IL-1β (f) in LPS-activated RAW 264.7 cells treated with IBP, PCA NPs or PCA@IBP NPs (n = 3). *p < 0.05, **p < 0.01, ***p < 0.001, and ****p < 0.0001.

Angiogenesis assay, designed to assess the formation of capillary-like structures by endothelial cells, is essential for assessing the pro-angiogenic potential of different treatments, particularly in wound healing and tissue regeneration contexts. Fig. 5a depicts the extent of tube formation (angiogenesis) at different time. Compared to IBP and control groups, more pronounced tube-shaped networks were visible in the PCA NPs and PCA@IBP NPs treated groups. According to the statistical data of Nb junctions and branches by ImageJ software (Fig. 5b–e), it illustrated that both PCA NPs and PCA@IBP NPs significantly enhanced angiogenesis compared to the control and IBP groups. The PCA@IBP NPs group showed the most pronounced pro-angiogenic effect at both 2 and 4 hours, as indicated by the number of junctions and branches formed. This suggested that PCA@IBP NPs had the optimum capacity to promote capillary structure formation, positioning them as a promising option for boosting vascularization in wound healing applications.

2.5 *In vivo* acute wound healing

Grounded in the outstanding *in vitro* results, we further evaluated the *in vivo* therapeutic efficacy of PCA@IBP NPs using an acute wound defect model. All animal procedures were performed in accordance with the Guidelines for Care and Use of Laboratory Animals of the Hong Kong University of Science and Technology (Guangzhou) and approved by the Institutional Animal Care and Use Committee (IACUC) of the Hong Kong University of Science and Technology (Guangzhou) with approval number HKUST(GZ)-IACUC-2024-A0044. Since the PCA@IBP NPs nanodrug delivery system was in liquid form, we further combined the PCA@IBP NPs delivery system with hyaluronic acid (HA), a natural extracellular matrix polysaccharide, to enhance its retention and attachment time at the wound site. Based on the unique viscoelastic properties and excellent biocompatibility of HA, the addition of HA could increase the viscosity of the wound dressing, thereby improv-

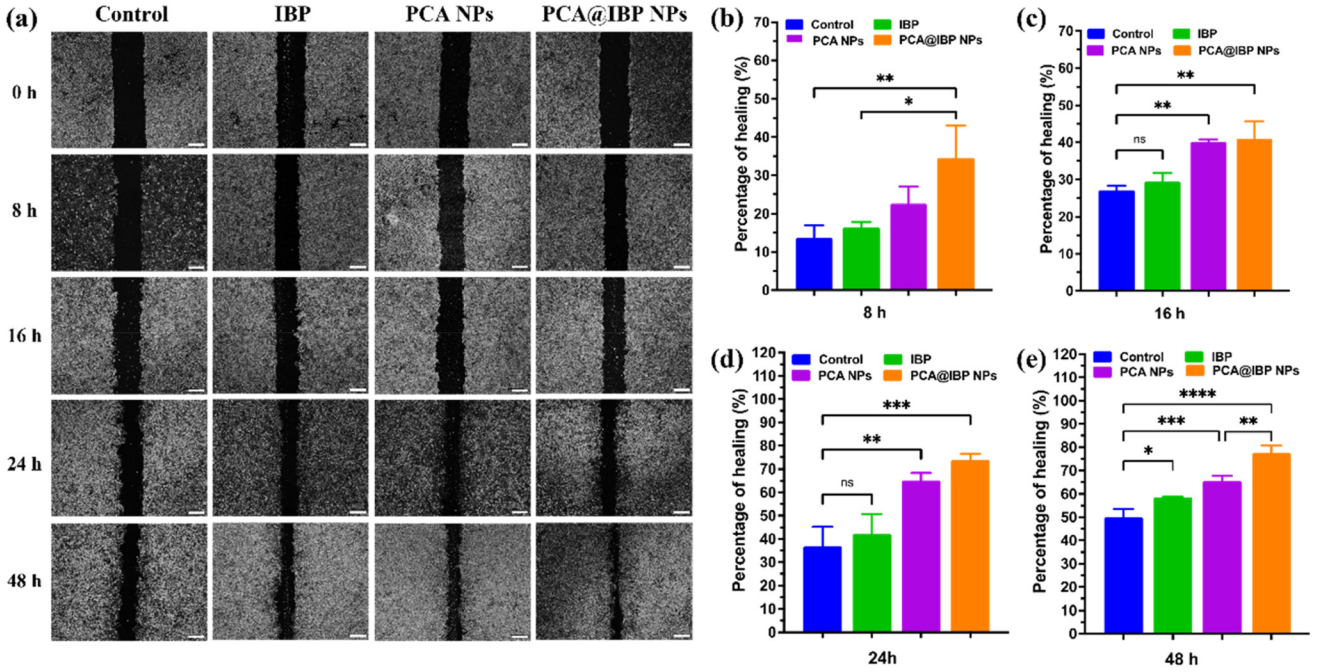

Fig. 4 *In vitro* scratch healing promotion of PCA@IBP NPs. (a) Representative images of cell migration of NIH 3T3 cells after specific treatment. Scale bar is 200 μm. (b–e) Quantitative analysis of wound healing ratio at 8 h, 16 h, 24 h and 48 h (n = 3). *p < 0.05, **p < 0.01, ***p < 0.001, ****p < 0.0001 and ns means no significant difference.

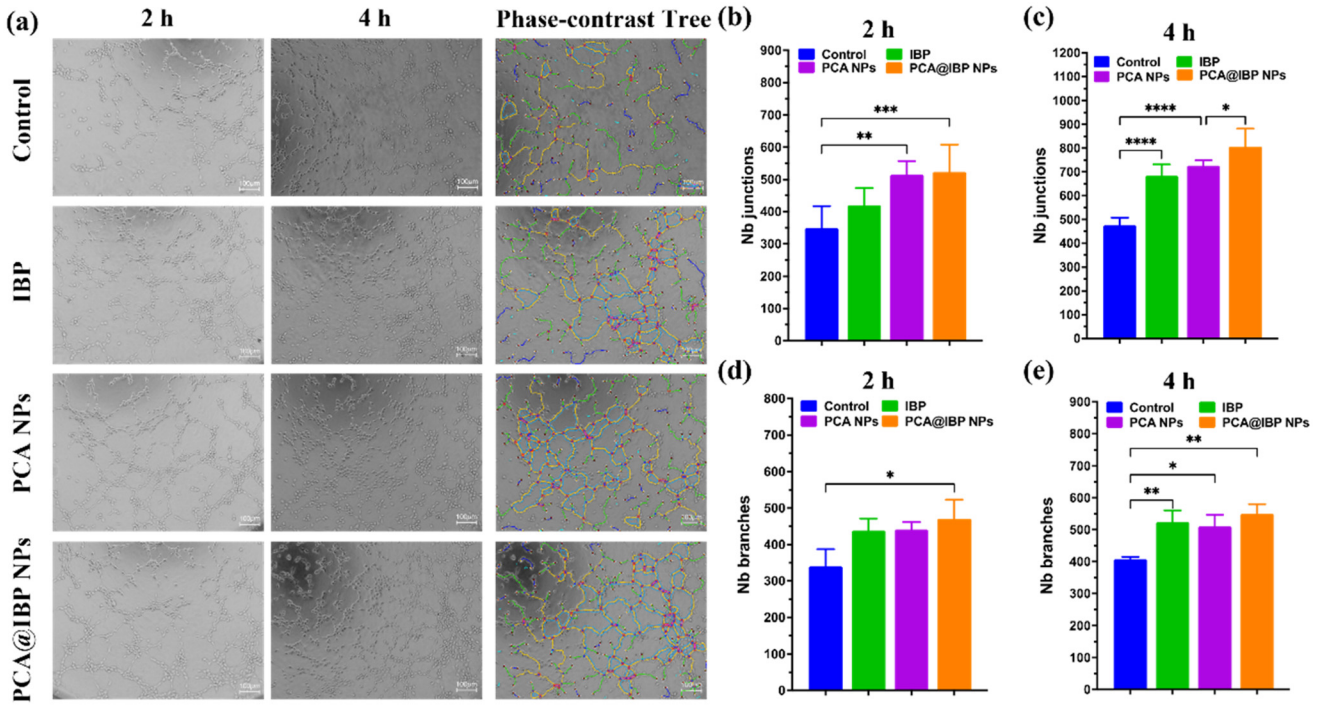

Fig. 5 *In vitro* pro-angiogenesis effects of PCA@IBP NPs. (a) The representative images of tube formation assays and phase-contrast tree analysis of endothelial network at 4 h. Scar bar = 100 μm. (b–e) Statistical results of Nb junctions and Nb branches in different times (n = 3). *p < 0.05, **p < 0.01, ***p < 0.001, and ****p < 0.0001.

ing the adhesion to the wound surface and extending the drug retention at the wound location. HA is quite accessible as one of the commonly used wound dressing candidates and meets our requirements for a simple wound dressing, thus it was selected as the representative of moisturizers and loading matrix in our study. Prolonging the sustained release and

action time of nanodrugs with the assistance of HA could better verify the therapeutic outcomes of PCA@IBP NPs in wound healing.

Here, the mice were categorized into five groups: (i) Saline treating as control group; (ii) HA group; (iii) IBP/HA group; (iv) PCA NPs/HA group; (v) PCA@IBP NPs/HA group. Fig. 6a illustrates the wound healing progress across five groups at days 7, 14, and 21. The wound area gradually decreased over time in all groups showing the healing ratio from each treating group. The treatment groups containing HA showed enhanced wound healing compared to the control group, consistent with the statistical analysis (Fig. 6b). Notably, the PCA@IBP NPs/HA group demonstrated the best healing efficacy at all time points. After 7 days of treatment, the PCA@IBP NPs/HA group showed 76% wound closure, while the control group exhibited 64% closure with significant differences already ($p < 0.05$). At day 14, the wounds in the PCA@IBP NPs/HA group had healed by 94%, also significantly different from that of the control group with 87% healing achieved ($p < 0.05$). After 21 days, the wounds in the PCA@IBP NPs/HA group were almost fully healed, but the control group still had visible wound areas ($p < 0.001$). The therapeutic efficacy of PCA@IBP NPs in acute wound treatment was not only manifested in the differential wound healing area (reflecting accelerated healing speed), but also demonstrated superior wound healing efficiency at the histological level. To further examine the internal tissue healing, H&E and Masson staining were performed (Fig. 6c and d), providing insights into the structural tissue repair and

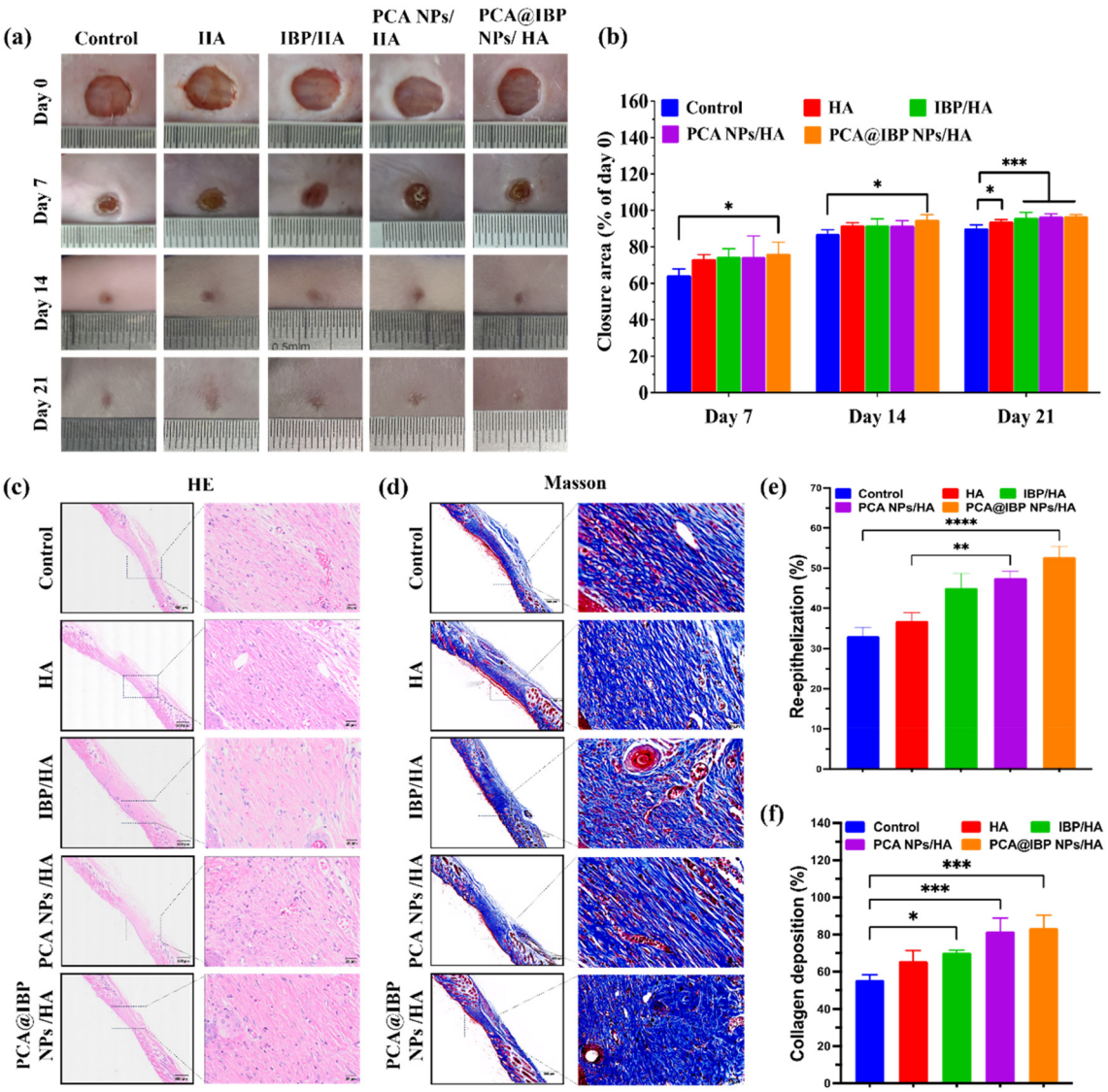

Fig. 6 The *in vivo* healing process and histologic analysis of acute wounds after various treatments. (a) Representative images of acute wound healing in mice. (b) Rates of the closure wound after day 7, day 14, and day 21 ($n = 3$). (c) Representative H&E staining and (d) Masson staining images from different groups. The statistical analysis of (e) re-epithelization and (f) collagen deposition according to the tissue section ($n = 3$). *$p < 0.05$, **$p < 0.01$, ***$p < 0.001$, and ****$p < 0.0001$.

collagen accumulation at the wound site. These analyses are crucial for understanding the extent of tissue repair at the microscopic level, complementing the visible wound closure observations. As illustrated in Fig. 6e, the PCA@IBP NPs/HA treatment group exhibited a significantly higher degree of re-epithelialization, indicating more advanced wound closure and tissue regeneration. Additionally, the PCA@IBP NPs/HA group showed improved collagen deposition, as evidenced in Masson staining. The enhanced collagen deposition suggested better structural integrity and tissue remodeling by PCA@IBP NPs/HA treatment, critical for effective wound healing (Fig. 6f). These results further confirmed the superior therapeutic potential of the PCA@IBP NPs/HA system, which promoted both re-epithelialization and collagen formation facili-

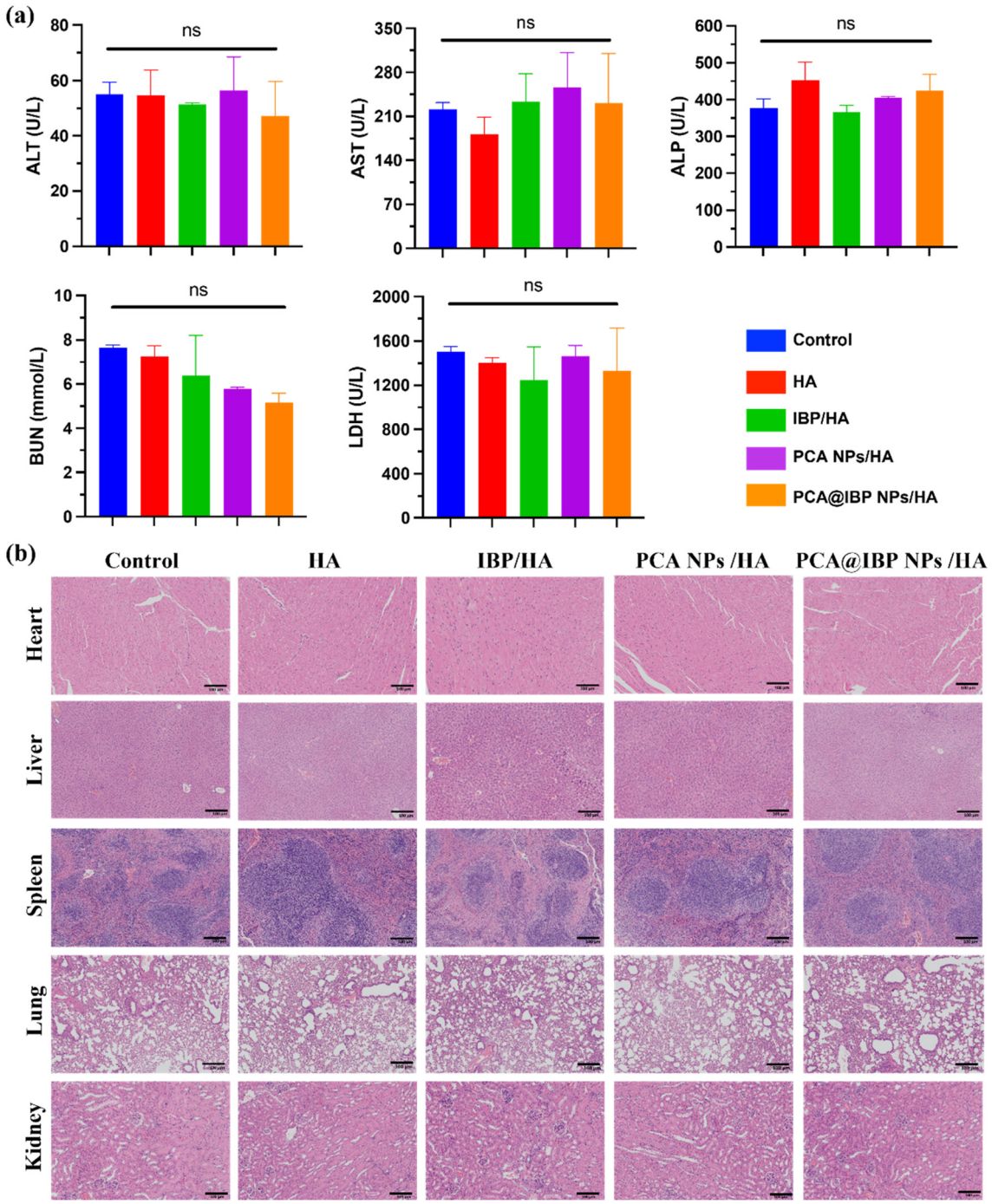

Fig. 7 The *in vivo* safety evaluation of NPs. (a) Levels of ALT, AST, ALP, BUN and LDH in serum collected from mice after acute wound healing (n = 3). (b) H&E staining of major organs collected from mice after acute wound healing. Scale bar is 100 μm. ns means no significant difference among groups.

tating accelerative wound repair and improved skin tissue regeneration.

2.6 *In vivo* safety evaluation

To assess the *in vivo* biocompatibility of the PCA@IBP NPs nanodrug delivery system, blood samples were collected from the mice at the end of the healing process for biochemical analysis. As shown in the Fig. 7a, no significant differences were observed in liver and kidney function markers among all the treating groups. At the same time, major organs including heart, liver, spleen, lungs and kidney were harvested for H&E staining. Fig. 7b demonstrated that no lesions or signs of inflammation were detected at the histological levels. These results reflected that PCA@IBP NPs exhibited satisfactory *in vivo* safety with minimal risk of systemic toxicity, indicating their high potential for broader biomedical applications.

3 Conclusion

In conclusion, the combination of PCA@IBP NPs with HA exhibited many substantial advantages for addressing acute wounds. The results from the acute wound model indicated that PCA@IBP NPs/HA significantly accelerated wound healing, promoting a higher degree of re-epithelialization and enhanced collagen deposition compared to the control and other groups. These findings aligned with the superior cell behavior observed *in vitro*, confirming the effectiveness of the PCA-based nanodrug system in supporting tissue regeneration and optimizing structural integrity mainly *via* anti-inflammation. The *in vivo* safety evaluation indicated little systematic toxicity of PCA@IBP NPs/HA treatment, thereby exhibiting excellent biocompatibility. Overall, the PCA@IBP NPs/HA nanodrug delivery system offered a promising and safe therapeutic approach for enhancing wound healing in acute wounds, with benefits in promoting tissue reconstruction and functional restoration. Furthermore, this novel multifunctional platform derived from natural bioactive herbal components would provide a new strategy for the clinical applications of wound treatment and care.

Author contributions

S. W. and L. W. designed and performed the experiments and wrote the paper; M. Y. performed supplemental experiments, data analysis and major revision of the manuscript; S. H. and X. Y. analyzed data, discussed the results and revised the paper; J. W. supervised, and leaded the projects.

Conflicts of interest

The authors declare no conflict of interest.

Data availability

The authors confirm that the data supporting the findings of this study are available within the article and its ESI.†

Acknowledgements

This research was accomplished with the support by National Natural Science Foundation of China (52173150), and the Guangzhou Science and Technology Program City-University Joint Funding Project (2023A03J0001), the Guangdong Basic and Applied Basic Research Foundation (2023A1515110463), the Shenzhen Science and Technology Program (JCYJ20240813150453070) and the Postdoctoral Fellowship Program of CPSF (GZC20233297).

References

1 R. Li, K. Liu, X. Huang, D. Li, J. Ding, B. Liu and X. Chen, *Adv. Sci.*, 2022, **9**, e2105152.
2 Y. Liang, J. He and B. Guo, *ACS Nano*, 2021, **15**, 12687–12722.
3 C. R. Wang, E. S. Sani, C. D. Shih, C. T. Lim, J. Wang, D. G. Armstrong and W. Gao, *Nat. Rev. Mater.*, 2024, **9**, 550–566.
4 T. Xiang, Q. R. Guo, L. H. Jia, T. Y. Yin, W. Huang, X. Y. Zhang and S. B. Zhou, *Adv. Healthcare Mater.*, 2024, **13**, 2301885.
5 R. Shaw, K. Patel, N. M. A. Chimthanawala, S. Sathaye and S. K. Maji, *Adv. Healthcare Mater.*, 2025, **14**, 2403560.
6 H. Ding, J. Yang, Y. Shuai, D. Wei, X. Liu, G. Li, L. Jin and J. Shen, *Chin. Chem. Lett.*, 2025, **36**, 110286.
7 A. G. Kurian, R. K. Singh, V. Sagar, J. H. Lee and H. W. Kim, *Nano-Micro Lett.*, 2024, **16**, 110.
8 S. L. Shang, K. T. Zhuang, J. W. Chen, M. Zhang, S. M. Jiang and W. Li, *Bioact. Mater.*, 2024, **34**, 298–310.
9 S. Liu, J. M. Yu, Y. C. Gan, X. Z. Qiu, Z. C. Gao, H. Wang, S. X. Chen, Y. Xiong, G. H. Liu, S. E. Lin, A. McCarthy, J. V. John, D. X. Wei and H. H. Hou, *Mil. Med. Res.*, 2023, **10**, 16.
10 P. Ye, Y. Yang, M. Z. Liu, J. Q. Meng, J. Y. Zhao, J. W. Zhao, J. H. Wang, Q. Y. Lu, J. Liu, L. Y. Wang, J. D. Lei and C. L. Wang, *Adv. Mater.*, 2025, **37**, 2419430.
11 C. Dai, L. Wang, X. You, Y. Zhao, Z. Cao and J. Wu, *Chin. Chem. Lett.*, 2025, **36**, 109869.
12 J. Guo, K. Su, L. Wang, B. Feng, X. You, M. Deng, W. S. Toh, J. Wu, B. Cheng and J. Xia, *Bioact. Mater.*, 2024, **40**, 212–226.
13 Y. Nie, L. Wang, S. Liu, C. Dai, T. Cui, Y. Lei, X. You, X. Wang, J. Wu and Z. Zheng, *J. Nanobiotechnol.*, 2023, **21**, 484.
14 Y. T. Wang, M. J. Ni, M. Y. Huang, L. Y. Xing, X. Liu, F. Y. Jia and Y. Huang, *Int. J. Pharm.*, 2025, **674**, 125439.

15 Y. Wang, C. F. Yang, W. G. Zhang, X. Y. Wang, Z. Zhao, Z. Y. Wang and L. L. Zhang, *Int. J. Biol. Macromol.*, 2025, **301**, 140326.
16 M. L. Song, Y. Y. Sun, H. J. Yin, Y. Li and H. Yang, *Acta Pharmacol. Sin.*, 2025, DOI: **10.1038/s41401-025-01510-0**.
17 Z. B. Li, H. J. Dong, S. Y. Yang, X. M. Wang and Z. Li, *Int. J. Nanomed.*, 2025, **20**, 4535–4550.
18 R. M. Khalil, E. S. Shalaby, M. F. Abdelhameed, M. E. Shabana and M. A. Wagdi, *J. Pharm. Sci.*, 2025, **114**, 103796.
19 Z. W. Lin, Y. L. Chen, W. L. Lei, C. Y. Ku, P. Y. Su, L. C. Tai, T. H. Tsai, Y. T. Liao, A. E. Y. Chuang and W. C. Huang, *J. Controlled Release*, 2025, **383**, 113760.
20 C. Y. Li, J. T. Wang, K. L. Liu, H. W. Ding, Q. F. Li, G. F. Liang, L. Jin and D. Y. He, *Chem. Eng. J.*, 2024, **493**, 152513.
21 X. L. Zhang, H. Li, Y. Liu, J. Yu, P. F. Zhang, P. L. Yu, Y. H. Liu, S. Jia, L. J. Ling, P. Li, L. Li, Y. Y. Wang, T. X. Huang, G. X. Jin, Y. P. Zhao, G. Ma, Q. H. Yuan, L. Zhu, Z. Y. Zhang, H. Li and W. W. Li, *Bioact. Mater.*, 2025, **44**, 269–282.
22 Y. C. Hu, J. C. Zhou, Y. H. Gao, Y. Fan, B. Chen, J. T. Su and H. Li, *Biomed. Mater.*, 2025, **20**, 032006.
23 M. X. Chen, T. Liu, X. N. Wang, L. Z. Gao, Y. Q. Cheng, J. Jiang and J. H. Zhang, *J. Nanobiotechnol.*, 2025, **23**, 342.
24 Y. H. Liu, X. X. Yang, K. F. Wu, J. Y. Feng, X. Zhang, A. Li, C. Cheng, Y. Z. Zhu, H. Guo and X. L. Wang, *Adv. Mater.*, 2025, **37**, 2414989.
25 R. F. Liu, E. R. Zhao, Y. J. Wang, H. Zuo, L. L. Li, Q. Y. Xia and H. W. He, *J. Nanobiotechnol.*, 2025, **23**, 11.
26 Y. Wang, Y. Zhang, Y. P. Yang, M. Y. Jin, S. Huang, Z. M. Zhuang, T. Zhang, L. L. Cao, X. Y. Lin, J. Chen, Y. Z. Du, J. Chen and W. Q. Tan, *Bioact. Mater.*, 2024, **35**, 330–345.
27 A. N. Bokatyi, N. Dubashynskaya and Y. A. Skorik, *Carbohydr. Polym.*, 2024, **337**, 122145.
28 T. Liu, G. Liu, J. Zhang, Z. Ding, Y. Li, K. Sigdel, X. Wang and H. Xie, *Chin. Chem. Lett.*, 2022, **33**, 1880–1884.
29 Z. Zhao, S. Han, W. Feng, Z. Zhang, S. Shen, H. Huang and J. Wu, *Int. J. Biol. Macromol.*, 2025, **300**, 140186.
30 B. Li, Q. X. Gao, Y. X. Wu, H. Y. Lei, S. C. Ma, W. Wang, H. Sun, W. F. Ma, J. D. Zheng, C. C. Yuan, Y. L. Zhang, Y. Jia, F. Ma, Q. Gu, S. Sang, H. Duan, H. M. Shi, X. T. Fu, G. T. Lu, Z. Y. Shan, Y. D. Jiang and Y. H. Liao, *Chem. Eng. J.*, 2025, **507**, 160643.
31 Z. Xu, B. Liang, J. Tian and J. Wu, *Biomater. Sci.*, 2021, **9**, 4388–4409.
32 Y. Yan, B. Li, Q. X. Gao, M. Wu, H. Ma, J. W. Bai, C. T. Ma, X. Y. Xie, Y. Gong, L. Q. Xu, X. X. Li, W. Wang, Y. Q. Wu, J. M. Wang, H. H. Wang, Y. Feng, Y. L. Zhang, P. R. Li, H. M. Shi, F. Ma, Y. Jia, H. Duan, X. T. Fu, W. Y. Wang, L. Y. Zhan, X. J. Du, H. T. Zhou and Y. H. Liao, *Adv. Sci.*, 2025, **12**, 2412799.
33 X. Y. Wang, R. Mu, Y. Zhou, J. M. Li, Q. L. Ma, J. Wang, Y. F. Ma, W. B. Sheng, X. Z. Hu, F. Zhou and B. Li, *Adv. Funct. Mater.*, 2025, 2423356.